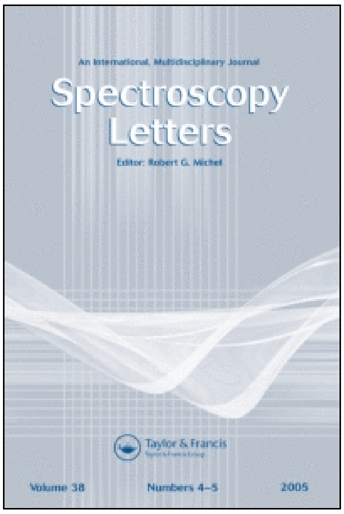

Spectroscopy Letters
Publication details, including instructions for authors and subscription information:
http://www.informaworld.com/smpp/title~content=t713597299

Comparative Investigation on the Excitation of Copper Emission Lines Between Argon and Helium Spark Discharge Plasmas

Syuya Nakamura[a]; Kazuaki Wagatsuma[a]
[a] Institute for Materials Research, Tohoku University, Sendai, Japan

To cite this Article Nakamura, Syuya and Wagatsuma, Kazuaki(2006) 'Comparative Investigation on the Excitation of Copper Emission Lines Between Argon and Helium Spark Discharge Plasmas', Spectroscopy Letters, 39: 5, 497 — 509
To link to this Article: DOI: 10.1080/00387010600851549
URL: http://dx.doi.org/10.1080/00387010600851549

Spectroscopy Letters, 39: 497–509, 2006

ISSN 0038-7010 print/1532-2289 online
DOI: 10.1080/00387010600851549

Comparative Investigation on the Excitation of Copper Emission Lines Between Argon and Helium Spark Discharge Plasmas

Syuya Nakamura and Kazuaki Wagatsuma
Institute for Materials Research, Tohoku University, Sendai, Japan

Abstract: The emission intensities and the signal-to-background ratios (SBRs) of copper emission lines in the wavelength range 200–360 nm were observed from a medium-voltage spark discharge plasma when argon or helium was employed as the surrounding gas. The observed copper spectra comprised Cu(I) lines having excitation energy of 3.8–9.3 eV, and Cu(II) lines assigned to three different transitions: $3d^84p$–$3d^84s$ transition (excitation energy of 8.2–9.2 eV), $3d^85s$–$3d^84p$ transition (13.4–13.6 eV), and the $3d^84d$–$3d^84p$ transition (14.2–14.8 eV). The Cu(I) lines have much smaller intensities in the helium plasma compared with the argon plasma, whereas the Cu(II) lines have similar intensities between both plasmas. The SBRs of some ionic copper lines are larger in the helium plasma compared with the argon plasma. Therefore, when an ionic line has to be measured in the analytical applications, the helium plasma should be recommended.

Keywords: Argon plasma, copper emission lines, helium plasma, signal-to-background ratio, spark discharge optical emission spectrometry

INTRODUCTION

Spark discharge optical emission spectrometry (SD-OES) is being extensively employed for the direct analysis of solid samples due to the rapid response as well as the capability of multielemental determination, and it thus has become a standard method in the on-site analysis for production control in metallurgical industries. Especially in steel-making processes, the content of

Received 23 January 2006, Accepted 9 June 2006
Address correspondence to Kazuaki Wagatsuma, Institute for Materials Research, Tohoku University, Katahira 2-1-1, Sendai 980-8577, Japan. E-mail: kwagatsuma@mm.neweb.ne.jp

the alloyed elements is required to be strictly controlled because it fundamentally determines the performance of steel materials. SD-OES plays an important role for monitoring the content variations during the refining process of manufactured steels. However, because refining techniques are recently advanced, impurity elements in steel can be reduced down to content ranges of several parts per million, which are in some cases below the detection limits of SD-OES. Therefore, the improvement in the analytical performance of SD-OES is required.

Fundamental studies on the emission characteristics of spark discharge plasmas were investigated in the 1960s,[1–3] which was followed by the development of modern equipment for SD-OES and the algorithm for data handling such as a pulse distribution analysis method.[4–6] The early detector system using a photographic plate was replaced with photomultiplier tubes in the modern equipment, leading to an advanced measurement in SD-OES using intensity integration for individual analytical lines and rapid computer-controlled data readout. Recent commercial spectrometric systems, which comprise a spark discharge source, a multichannel spectrometer, and a computer for data treatment, are available from several manufacturers. More recently, few studies on the fundamental processes occurring in a spark discharge plasma were reported, probably because experimental parameters of spark discharge might have been optimized completely in early scientific papers. However, solid-state detectors such as an intensified charge-coupled device (ICCD) detector now may improve the detection system in SD-OES, which enables the spark discharge plasma to be observed in more detail; it is easy to obtain the spark discharge spectrum and to estimate the emission intensities of many spectral lines accurately. Such progress of the equipment for SD-OES will help one to re-examine spark discharge plasmas with respect to fundamental research on the excitation mechanisms as well as further optimization of the experimental conditions in the analytical applications.

In this paper, the details of copper emission spectra excited by spark discharge plasmas are compared when argon or helium is used as the surrounding gas. The emission intensities of copper atomic or ionic lines having various excitation energies were measured by using these spark discharge plasmas. Compared with the atomic lines, the relative emission intensity of the ionic lines is enhanced in the helium plasma, and this effect becomes more prominent with increasing excitation energies. The excitation mechanism of copper lines is suggested from these experiments.

MATERIALS AND METHODS

Transient Response of Spark Discharge Plasma

As shown in Fig. 1, the spark discharge plasma is temporally and spatially changed with the progress of a spark. During the formation of a spark

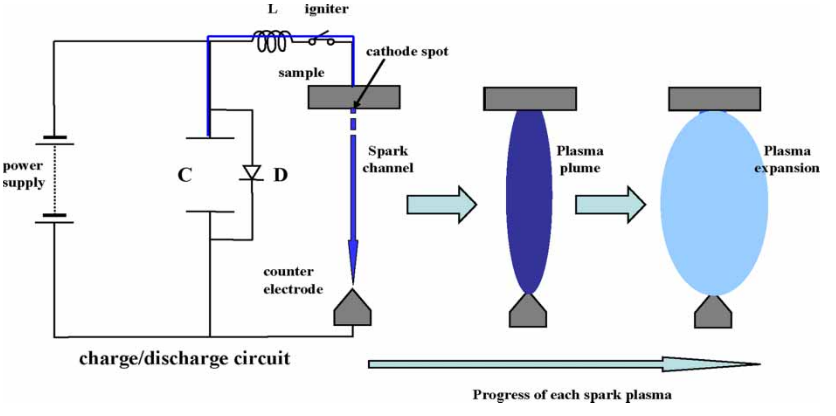

Figure 1. Model of the transient process occurring in spark discharge plasma.

discharge, a spark channel is first built, and then a plasma plume is produced by several cathode spots appearing at the cathode. In the spark channel, sample species ejected from the cathode as well as gas species receive energies through collisions with the fast electrons. In the plasma plume, in addition to the fast electrons, secondary electrons that are produced through collisions with fast electrons and excited species of the plasma gas having kinetic and/or internal energies can contribute to the excitations of the sample atoms. Immediately after the discharge of the capacitor, few electrons leave in the plasma plume because the recombination of electrons occurs rapidly. However, it is possible to excite the sample atoms through collisions with energetic gas species, which are called metastable states, even during the expansion of the plasma plume. One always observes intense continuum radiation resulting from deacceleration collisions of fast electrons with gas species in the initial stage of the spark discharge, which may hinder the measurement of the emission intensity of sample analytical lines accurately when it becomes very faint. In the expansion stage of the spark plasma, the contribution from the continuum radiation decreases, although the direct energy transfer from the spark discharge is reduced. These effects can be estimated from the signal-to-background ratio (SBR) of the analytical lines under various discharge conditions. The kind of plasma gas and the pressure are predominant experimental parameters for determining the interaction between fast electrons from the discharge circuit and gas species working as the energy receiver. It is thus considered that the optimization of these parameters should be performed in SD-OES.

Apparatus and the Operating Conditions

A spark discharge emission source (model PDA-5520 II, Shimadzu Corp., Shimoto, Japan) was employed, where the original discharge chamber was replaced with a laboratory-made chamber having vacuum-sealed ports so that the plasma gas and the pressures could be strictly controlled during the discharges. In this study, spark discharges were conducted under ambient pressure conditions of pure argon (99.9995%, purity) or of pure helium (99.9999%, purity). The discharge voltage was 500 V, and the frequency of the spark shots were preset to be 500 Hz. The sample was a pure copper plate (99.99%, purity) and the counterelectrode was made from tungsten, where the distance between these electrodes was kept at 4 mm.

After a predischarge period of 3 s, the emission spectra from the spark plasmas were recorded on a spectrograph (model MS-3504, SOLAR TII, Tokyo, Japan) equipped with an ICCD detector (model DH501-18F-03, Andor, South Windsor, CT, USA). Using the argon and helium plasmas, each set of the emission spectrum in the wavelength interval of 20 nm was recorded over the wavelength range 200–360 nm. The gate width of the detector was selected to be 0.5 s, meaning that averaging of the emission intensities over 250 spark shots was conducted in each spectrum. The whole image of each spark plasma could be integrated by using fiberoptics with the acceptance angle of about 12.5 degrees.

RESULTS AND DISCUSSION

Many emission lines of neutral and singly ionized copper were observed in the wavelength range 200–360 nm when argon or helium was employed as the plasma gas. The atomic lines are identified to various electronic transitions having excitation energy of 3.8–9.3 eV and the ionic lines to three different transitions: $3d^84p$–$3d^84s$ transition (excitation energy of 8.2–9.2 eV), $3d^85s$–$3d^84p$ transition (13.4–13.6 eV), and the $3d^84d$–$3d^84p$ transition (14.2–14.8 eV). Their assignment was estimated from the literature data regarding copper energy levels.[7]

Figure 2 shows spectral scans of copper emitted from the argon plasma (lower) and the helium plasma (upper) in the wavelength range 319–339 nm, where all of the observed emission lines, including two atomic resonance lines, Cu(I) 324.75 nm (3.78 eV) and Cu(I) 327.40 nm (3.84 eV), are assigned to neutral copper atom. Atomic lines of copper having larger excitation energies also appear in this wavelength region. Their emission intensities for the argon plasma are 15 times or more larger than those for the helium plasma. For instance, the intensity ratio of the helium plasma to the argon plasma is 0.068 for Cu(I) 327.40 nm (3.79 eV), 0.058 for Cu(I) 327.98 nm (5.42 eV), 0.071 for Cu(I) 329.05 nm (8.84 eV), and 0.068 for Cu(I) 330.80 nm (8.82 eV), indicating that their intensity ratios are almost constant against the excitation energy. On the other hand, ionic copper lines yield different variations in the emission intensity from the atomic lines. Figure 3 shows the copper spectra in the wavelength range 239–259 nm, where most of the emission lines are identified to the $3d^84p$–$3d^84s$ or the $3d^85s$–$3d^84p$ transitions of copper ion. These ionic lines

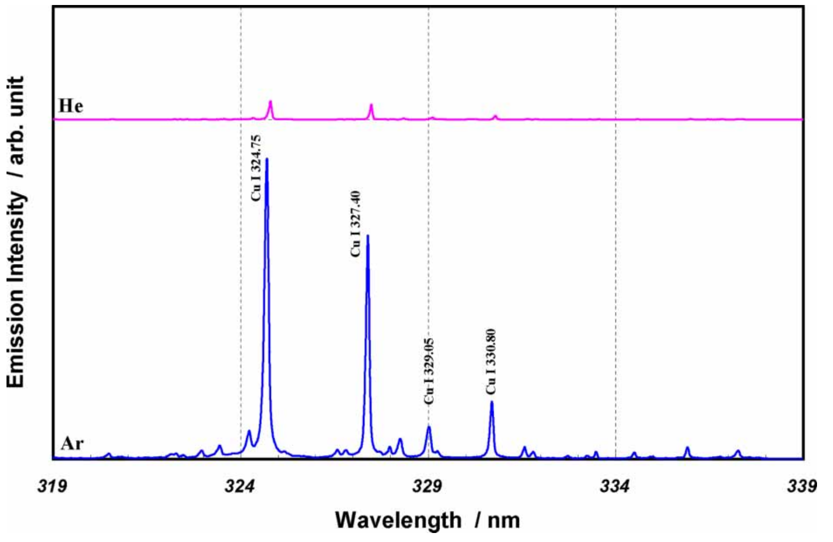

Figure 2. Spectral scans of copper sample emitted from helium (upper) and argon (lower) spark discharge plasmas in the wavelength range 319–339 nm.

emitted from the helium plasma have similar emission intensities to the corresponding lines from the argon plasma, and their relative intensities are elevated with increasing excitation energy. For instance, the intensity ratio of the helium plasma to the argon plasma is 0.44 for Cu(II) 240.01 nm (8.42 eV), 0.47 for

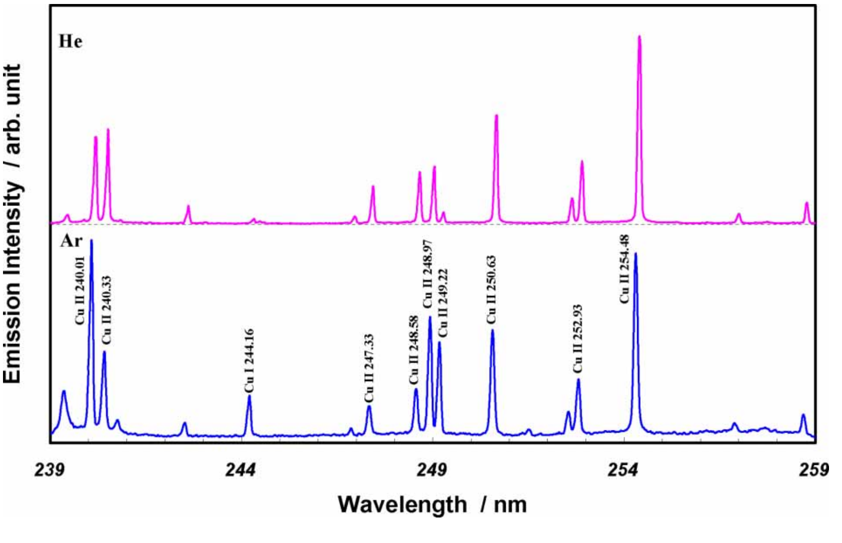

Figure 3. Spectral scans of copper sample emitted from helium (upper) and argon (lower) spark discharge plasmas in the wavelength range 239–259 nm.

Cu(II) 248.97 nm (8.23 eV), 1.02 for Cu(II) 250.63 nm (13.43 eV), and 1.02 for Cu(II) 254.48 nm (13.39 eV). It should be noted that, also in this wavelength region, atomic lines such as Cu(I) 244.16 nm and Cu(I) 249.22 nm have much smaller intensities in the helium plasma.

Table 1 summarizes emission lines of copper observed in the wavelength range 200–360 nm, together with their emission intensities for the argon and the helium plasmas. The emission intensity was estimated by integrating each net intensity for 0.5 s on an arbitrary scale. Figure 4 shows variations in the intensity ratio of the helium plasma to the argon plasma as a function of the energy sum for excitation (the total energy for the ionization and the excitation in the case of ionic lines). The intensity ratios for the atomic lines are small and almost independent of the excitation energy, whereas the ratios for the ionic lines are elevated with increasing excitation energy although large deviations of these intensity data are observed.

Figure 5 shows wavelength dependence of the background levels (intensity), which are measured at wavelength positions including no spectral lines, in the argon and the helium plasmas. The background levels for both plasmas are elevated with the wavelengths and give much larger values in the argon plasma compared with the helium plasma. For instance, the ratio of the background intensity of the helium plasma to the argon plasma is 0.32 at 207 nm, 0.18 at 232 nm, 0.12 at 261 nm, 0.086 at 294.5 nm, 0.056 at 316.5 nm, 0.054 at 321 nm, and 0.055 at 343 nm. The background ratio becomes larger with increasing wavelength, because the background level for the argon plasma is relatively higher at larger wavelengths. These effects can be explained by a difference in the stopping power (cross section) of inelastic collision between argon and helium with fast electrons, because continuum background radiation principally results from deacceleration collisions of fast electrons with gas species. It is well-known that the stopping power of helium atom is much smaller compared with argon atom. Therefore, fast electrons would run through a helium gas cloud with little loss of their kinetic energies; thus, the background intensity becomes smaller in the helium plasma, which means that the energy transfer from fast electrons to plasma gas species is insufficient in the helium plasma rather than the argon plasma, especially in the initial stage of the spark discharge. This phenomenon also exerts a negative effect on the excitation processes in the expansion stage of the spark plasma because direct energy transfer from the spark discharge is reduced. It is expected that the amounts of samples ejected from the cathode decrease in the helium plasma because the cathode spots cannot be grown sufficiently. In fact, it was observed that the crater depth on the sample surface in helium atmosphere was much smaller than that in argon, implying that smaller amounts of copper atom were introduced in the helium plasma, although quantitative determination was not performed. The behavior of the atomic lines in Fig. 4 would be explained by the difference in the sampling amounts of copper between using argon and helium gas. Because the atomic lines can be emitted through various collisional

Table 1. Observed emission lines in argon and helium spark discharge plasmas

Wavelength (nm)	Assignment		Relative intensity	
	Upper (eV)	Lower (eV)	Ar	He
Cu(II) 199.969	$4p\ ^{1}\mathbf{F}_{3}$ (8.9167)	$4s\ ^{3}\mathbf{D}_{3}$ (2.7187)	4200	2100
Cu(I) 202.434	$5p\ ^{2}\mathbf{P}_{1/2,3/2}$ (6.1226)	$4s\ ^{2}\mathbf{S}_{1/2}$ (0.0000)	3300	1500
Cu(II) 202.548	$4p\ ^{1}\mathbf{D}_{2}$ (9.0945)	$4s\ ^{3}\mathbf{D}_{1}$ (2.9753)		
Cu(II) 203.713	$4p\ ^{1}\mathbf{F}_{3}$ (8.9167)	$4s\ ^{3}\mathbf{D}_{2}$ (2.8326)	4800	2500
Cu(II) 204.379	$4p\ ^{3}\mathbf{D}_{3}$ (8.7830)	$4s\ ^{3}\mathbf{D}_{3}$ (2.7187)	6100	2900
Cu(II) 205.497	$4p\ ^{3}\mathbf{D}_{2}$ (8.8639)	$4s\ ^{3}\mathbf{D}_{2}$ (2.8326)	5500	2700
Cu(II) 208.530	$4p\ ^{3}\mathbf{F}_{2}$ (8.6623)	$4s\ ^{3}\mathbf{D}_{3}$ (2.7187)	1600	900
Cu(II) 208.792	$4d\ ^{3}\mathbf{G}_{3}$ (14.5985)	$4p\ ^{3}\mathbf{F}_{2}$ (8.6623)	1600	2000
Cu(II) 209.873	$4d\ ^{3}\mathbf{D}_{3}$ (14.3918)	$4p\ ^{3}\mathbf{F}_{3}$ (8.4862)	1300	1500
Cu(II) 210.479	$4p\ ^{3}\mathbf{D}_{2}$ (8.8639)	$4s\ ^{3}\mathbf{D}_{1}$ (2.9753)	6800	3300
Cu(II) 211.210	$4p\ ^{1}\mathbf{P}_{1}$ (9.1245)	$4s\ ^{1}\mathbf{D}_{2}$ (3.2563)	11000	4700
Cu(II) 211.837	$4d\ ^{3}\mathbf{P}_{2}$ (14.3371)	$4s\ ^{3}\mathbf{F}_{3}$ (8.4863)	3700	3400
Cu(II) 212.297	$4p\ ^{1}\mathbf{D}_{2}$ (9.0945)	$4s\ ^{1}\mathbf{D}_{2}$ (3.2563)	12000	5300
Cu(II) 212.604	$4p\ ^{3}\mathbf{F}_{2}$ (8.6623)	$4s\ ^{3}\mathbf{D}_{2}$ (2.8326)	13000	4800
Cu(II) 213.598	$4p\ ^{3}\mathbf{F}_{4}$ (8.5213)	$4s\ ^{3}\mathbf{D}_{3}$ (2.7187)	28000	11000
Cu(II) 214.879	$4p\ ^{3}\mathbf{F}_{3}$ (8.4862)	$4s\ ^{3}\mathbf{D}_{3}$ (2.7187)	15000	5600
Cu(II) 215.180	$4d\ ^{3}\mathbf{F}_{3}$ (14.4223)	$4p\ ^{3}\mathbf{F}_{2}$ (8.6624)	2300	1600
Cu(II) 216.132	$4d\ ^{3}\mathbf{G}_{3}$ (14.5985)	$4p\ ^{3}\mathbf{D}_{2}$ (8.8639)	2100	1600
Cu(I) 216.510	$4p\ ^{2}\mathbf{D}_{3/2}$ (5.7246)	$4s\ ^{2}\mathbf{S}_{1/2}$ (0.0000)	5700	400
Cu(II) 217.498	$4d\ ^{1}\mathbf{G}_{4}$ (14.6153)	$4p\ ^{1}\mathbf{F}_{3}$ (8.9167)	4300	3800
Cu(I) 217.895	$4p\ ^{2}\mathbf{P}_{3/2}$ (5.6882)	$4s\ ^{2}\mathbf{S}_{1/2}$ (0.0000)		
Cu(II) 217.940	$4p\ ^{3}\mathbf{F}_{2}$ (8.6623)	$4s\ ^{3}\mathbf{D}_{1}$ (2.9753)	35000	10000
Cu(I) 218.173	$4p\ ^{2}\mathbf{P}_{1/2}$ (5.6810)	$4s\ ^{2}\mathbf{S}_{1/2}$ (0.0000)	9600	1200
Cu(II) 218.963	$4p\ ^{1}\mathbf{F}_{3}$ (8.9167)	$4s\ ^{1}\mathbf{D}_{2}$ (3.2563)	26000	11000
Cu(II) 219.226	$4p\ ^{3}\mathbf{F}_{3}$ (8.4862)	$4s\ ^{3}\mathbf{D}_{2}$ (2.8326)	48000	32000
Cu(II) 219.567	$4d\ ^{3}\mathbf{F}_{4}$ (14.4279)	$4p\ ^{3}\mathbf{D}_{3}$ (8.7830)	7400	8800
Cu(I) 219.958	$4p\ ^{2}\mathbf{D}_{5/2}$ (7.0237)	$4s\ ^{2}\mathbf{D}_{5/2}$ (1.3889)	42000	11000
Cu(I) 219.975	$4p\ ^{2}\mathbf{D}_{3/2}$ (7.2766)	$4s\ ^{2}\mathbf{D}_{3/2}$ (1.6422)		
Cu(II) 220.057	$4d\ ^{3}\mathbf{F}_{2}$ (14.6958)	$4p\ ^{3}\mathbf{D}_{1}$ (9.0633)		
Cu(II) 221.026	$4p\ ^{3}\mathbf{D}_{2}$ (8.8639)	$4s\ ^{1}\mathbf{D}_{2}$ (3.2563)	35000	27000
Cu(I) 221.458	$4p\ ^{2}\mathbf{P}_{3/2}$ (6.9856)	$4s\ ^{2}\mathbf{D}_{5/2}$ (1.3889)	30000	12000
Cu(II) 221.510	$4d\ ^{1}\mathbf{F}_{3}$ (14.6898)	$4p\ ^{1}\mathbf{D}_{2}$ (9.0944)		
Cu(I) 221.566	$4p\ ^{2}\mathbf{P}_{1/2}$ (7.2361)	$4s\ ^{2}\mathbf{D}_{3/2}$ (1.6422)		
Cu(II) 221.599	$4d\ ^{3}\mathbf{F}_{3}$ (14.4617)	$4p\ ^{3}\mathbf{F}_{3}$ (8.8686)		
Cu(II) 221.810	$4p\ ^{3}\mathbf{P}_{1}$ (8.4204)	$4s\ ^{3}\mathbf{D}_{2}$ (2.8326)	43000	29000
Cu(I) 222.571	$4p\ ^{4}\mathbf{D}_{1/2}$ (5.5687)	$4s\ ^{2}\mathbf{S}_{1/2}$ (0.0000)		
Cu(II) 222.678	$4d\ ^{3}\mathbf{D}_{2}$ (14.4299)	$4p\ ^{3}\mathbf{D}_{2}$ (8.8639)		
Cu(I) 222.778	$4p\ ^{2}\mathbf{F}_{5/2}$ (7.2057)	$4s\ ^{2}\mathbf{D}_{3/2}$ (1.6422)		
Cu(II) 222.887	$4p\ ^{3}\mathbf{P}_{0}$ (8.5361)	$4s\ ^{3}\mathbf{D}_{1}$ (2.9754)	53000	22000
Cu(II) 222.985	$4d\ ^{3}\mathbf{F}_{3}$ (14.4223)	$4p\ ^{3}\mathbf{D}_{2}$ (8.8639)		
Cu(I) 223.009	$4p\ ^{2}\mathbf{F}_{7/2}$ (6.9467)	$4s\ ^{2}\mathbf{D}_{5/2}$ (1.3889)		

(*continued*)

Table 1. Continued

Wavelength (nm)	Assignment		Relative intensity	
	Upper (eV)	Lower (eV)	Ar	He
Cu(II) 224.261	*4p* $^{3}\mathbf{D}_{3}$ (8.7830)	*4s* $^{1}\mathbf{D}_{2}$ (3.2563)	48000	33000
Cu(II) 224.699	*4p* $^{3}\mathbf{P}_{2}$ (8.2347)	*4s* $^{3}\mathbf{D}_{3}$ (2.7187)	60000	38000
Cu(I) 226.308	*7p* $^{2}\mathbf{P}_{1/2}$ (7.1189)	*4s* $^{2}\mathbf{D}_{3/2}$ (1.6422)	8500	6200
Cu(II) 226.320	*4d* $^{3}\mathbf{P}_{1}$ (14.3404)	*4p* $^{3}\mathbf{D}_{2}$ (8.8639)		
Cu(II) 226.456	*4d* $^{3}\mathbf{P}_{2}$ (14.3371)	*4p* $^{3}\mathbf{D}_{2}$ (8.8639)		
Cu(II) 227.626	*4p* $^{3}\mathbf{P}_{1}$ (8.4204)	*4s* $^{3}\mathbf{D}_{1}$ (2.9754)	22000	18000
Cu(II) 229.436	*4p* $^{3}\mathbf{P}_{2}$ (8.2347)	*4s* $^{3}\mathbf{D}_{2}$ (2.8326)	36000	21000
Cu(I) 230.312	*4p* $^{2}\mathbf{D}_{5/2}$ (7.0237)	*4s* $^{2}\mathbf{D}_{3/2}$ (1.6422)	3600	700
Cu(II) 235.664	*4p* $^{3}\mathbf{P}_{2}$ (8.2347)	*4s* $^{3}\mathbf{D}_{1}$ (2.9753)	4900	3600
Cu(II) 236.989	*4p* $^{3}\mathbf{F}_{3}$ (8.4862)	*4s* $^{1}\mathbf{D}_{2}$ (3.2563)	42000	33000
Cu(I) 239.264	*6p* $^{4}\mathbf{P}_{1/2}$ (6.8224)	*4s* $^{2}\mathbf{D}_{3/2}$ (1.6422)	4100	800
Cu(II) 240.011	*4p* $^{3}\mathbf{P}_{1}$ (8.4204)	*4s* $^{1}\mathbf{D}_{2}$ (3.2563)	18000	7800
Cu(II) 240.334	*5s* $^{3}\mathbf{D}_{3}$ (13.3918)	*4p* $^{3}\mathbf{P}_{2}$ (8.2347)	7900	8600
Cu(I) 240.668	*6p* $^{2}\mathbf{P}_{3/2}$ (6.7922)	*4s* $^{2}\mathbf{D}_{3/2}$ (1.6422)	1500	300
Cu(II) 242.442	*5s* $^{3}\mathbf{D}_{1}$ (13.6484)	*4p* $^{3}\mathbf{P}_{0}$ (8.5361)	1200	1600
Cu(I) 244.164	*4p* $^{4}\mathbf{P}_{1/2}$ (5.0763)	*4s* $^{2}\mathbf{S}_{1/2}$ (0.0000)	3700	400
Cu(II) 247.333	*5s* $^{3}\mathbf{D}_{2}$ (13.4316)	*4p* $^{3}\mathbf{P}_{1}$ (8.4204)	2700	3400
Cu(II) 248.579	*5s* $^{3}\mathbf{D}_{1}$ (13.6484)	*4p* $^{3}\mathbf{F}_{2}$ (8.6623)	4300	4700
Cu(II) 248.966	*4p* $^{3}\mathbf{P}_{2}$ (8.2347)	*4s* $^{1}\mathbf{D}_{2}$ (3.2563)	11000	5100
Cu(I) 249.215	*4p* $^{4}\mathbf{P}_{3/2}$ (4.9734)	*4s* $^{4}\mathbf{S}_{1/2}$ (0.0000)	8600	1000
Cu(II) 250.626	*5s* $^{3}\mathbf{D}_{2}$ (13.4316)	*4p* $^{3}\mathbf{F}_{3}$ (8.4862)	9700	9900
Cu(II) 252.659	*5s* $^{3}\mathbf{D}_{3}$ (13.3918)	*4p* $^{3}\mathbf{F}_{3}$ (8.4862)	2200	2300
Cu(II) 252.930	*5s* $^{1}\mathbf{D}_{2}$ (13.6834)	*4p* $^{3}\mathbf{D}_{3}$ (8.7831)	5200	5700
Cu(II) 254.480	*5s* $^{3}\mathbf{D}_{3}$ (13.3918)	*4p* $^{3}\mathbf{F}_{4}$ (8.5213)	17000	17000
Cu(II) 259.053	*5s* $^{3}\mathbf{D}_{1}$ (13.6484)	*4p* $^{3}\mathbf{D}_{2}$ (8.8639)	2800	2600
Cu(II) 259.881	*5s* $^{3}\mathbf{D}_{2}$ (13.4316)	*4p* $^{3}\mathbf{F}_{2}$ (8.6623)	5200	4800
Cu(II) 260.026	*5s* $^{1}\mathbf{D}_{2}$ (13.6834)	*4p* $^{1}\mathbf{F}_{3}$ (8.9168)	8700	7600
Cu(I) 261.837	*5p* $^{2}\mathbf{P}_{3/2}$ (6.1226)	*4s* $^{2}\mathbf{D}_{5/2}$ (1.3889)	31000	3000
Cu(II) 266.629	*5s* $^{3}\mathbf{D}_{2}$ (13.4316)	*4p* $^{3}\mathbf{D}_{3}$ (8.7830)	2200	1900
Cu(II) 268.930	*5s* $^{3}\mathbf{D}_{3}$ (13.3918)	*4p* $^{3}\mathbf{D}_{3}$ (8.7830)	10000	9100
Cu(II) 270.097	*5s* $^{1}\mathbf{D}_{2}$ (13.6834)	*4p* $^{1}\mathbf{D}_{2}$ (9.0945)	11000	9900
Cu(II) 270.318	*5s* $^{3}\mathbf{D}_{1}$ (13.6484)	*4p* $^{3}\mathbf{D}_{1}$ (9.0633)	7200	6600
Cu(II) 271.351	*5s* $^{3}\mathbf{D}_{2}$ (13.4316)	*4p* $^{3}\mathbf{D}_{2}$ (8.8639)	11000	10000
Cu(II) 271.877	*5s* $^{1}\mathbf{D}_{2}$ (13.6834)	*4p* $^{1}\mathbf{P}_{1}$ (9.1246)	8300	6900
Cu(II) 272.167	*5s* $^{3}\mathbf{D}_{1}$ (13.6484)	*4p* $^{1}\mathbf{D}_{2}$ (9.0944)	3800	3300
Cu(II) 274.528	*5s* $^{3}\mathbf{D}_{2}$ (13.4316)	*4p* $^{1}\mathbf{F}_{3}$ (8.9168)	2800	2600
Cu(I) 274.954	*5s* $^{2}\mathbf{D}_{5/2}$ (8.3244)	*4p* $^{2}\mathbf{P}_{3/2}$ (3.8166)	3500	200
Cu(I) 276.639	*5p* $^{2}\mathbf{P}_{1/2,3/2}$ (6.1226)	*4s* $^{2}\mathbf{D}_{3/2}$ (1.6422)	18000	1500
Cu(II) 276.967	*5s* $^{3}\mathbf{D}_{3}$ (13.3918)	*4p* $^{1}\mathbf{F}_{3}$ (8.9167)	19000	12000
Cu(I) 282.437	*4p* $^{2}\mathbf{D}_{5/2}$ (5.7773)	*4s* $^{2}\mathbf{D}_{5/2}$ (1.3889)	44000	2900
Cu(II) 283.737	*5s* $^{3}\mathbf{D}_{2}$ (13.4316)	*4p* $^{3}\mathbf{D}_{1}$ (9.0633)	2900	2700

(*continued*)

Table 1. Continued

Wavelength (nm)	Assignment		Relative intensity	
	Upper (eV)	Lower (eV)	Ar	He
Cu(I) 285.873	$4p\ ^2\mathbf{D}_{3/2}$ (5.7246)	$4s\ ^2\mathbf{D}_{5/2}$ (1.3889)	2000	300
Cu(II) 287.770	$5s\ ^3\mathbf{D}_2$ (13.4316)	$4p\ ^1\mathbf{P}_1$ (9.1245)	4200	3200
Cu(I) 288.293	$4p\ ^2\mathbf{P}_{3/2}$ (5.6882)	$4s\ ^2\mathbf{D}_{5/2}$ (1.3889)	5800	300
Cu(I) 296.117	$4p\ ^2\mathbf{F}_{7/2}$ (5.5746)	$4s\ ^2\mathbf{D}_{5/2}$ (1.3889)	42000	2800
Cu(I) 299.839	$4p\ ^4\mathbf{D}_{3/2}$ (5.5226)	$4s\ ^2\mathbf{D}_{5/2}$ (1.3889)	5900	400
Cu(I) 301.082	$4p\ ^4\mathbf{D}_{5/2}$ (5.5055)	$4s\ ^2\mathbf{D}_{5/2}$ (1.3889)	14000	700
Cu(I) 301.201	$4d\ ^4\mathbf{F}_{5/2}$ (9.0884)	$4p\ ^4\mathbf{P}_{3/2}$ (4.9734)	2300	100
Cu(I) 302.152	$4d\ ^2\mathbf{D}_{3/2}$ (8.9396)	$4p\ ^4\mathbf{P}_{5/2}$ (4.8376)	6600	300
Cu(I) 302.260	$4d\ ^4\mathbf{F}_{7/2}$ (8.9382)	$4p\ ^4\mathbf{P}_{5/2}$ (4.8376)		
Cu(I) 302.499	$4d\ ^4\mathbf{D}_{5/2}$ (8.9350)	$4p\ ^4\mathbf{P}_{5/2}$ (4.8376)	2600	100
Cu(I) 303.610	$4p\ ^2\mathbf{D}_{3/2}$ (5.7246)	$4s\ ^2\mathbf{D}_{3/2}$ (1.6422)	13000	800
Cu(I) 306.341	$4p\ ^2\mathbf{P}_{3/2}$ (5.6882)	$4s\ ^2\mathbf{D}_{3/2}$ (1.6422)	13000	800
Cu(I) 307.380	$4p\ ^2\mathbf{F}_{5/2}$ (5.4212)	$4s\ ^2\mathbf{D}_{5/2}$ (1.3889)	3300	200
Cu(I) 308.812	$4d\ ^4\mathbf{F}_{3/2}$ (9.0899)	$4p\ ^4\mathbf{P}_{1/2}$ (5.0763)	4000	200
Cu(I) 309.398	$4p\ ^4\mathbf{D}_{7/2}$ (5.3949)	$4s\ ^2\mathbf{D}_{5/2}$ (1.3889)	5700	300
Cu(I) 309.992	$4d\ ^4\mathbf{D}_{7/2}$ (8.8359)	$4p\ ^4\mathbf{P}_{5/2}$ (4.8376)	21000	1100
Cu(I) 310.811	$5s\ ^4\mathbf{D}_{5/2}$ (7.8044)	$4p\ ^2\mathbf{P}_{3/2}$ (3.8166)	41000	2100
Cu(I) 311.635	$4d\ ^2\mathbf{D}_{5/2}$ (8.8148)	$4p\ ^4\mathbf{P}_{5/2}$ (4.8376)	11000	600
Cu(I) 312.047	$4d\ ^2\mathbf{F}_{5/2}$ (8.9454)	$4p\ ^4\mathbf{P}_{3/2}$ (4.9734)	3100	100
Cu(I) 312.499	$4d\ ^2\mathbf{D}_{3/2}$ (8.9396)	$4p\ ^4\mathbf{P}_{3/2}$ (4.9734)	38000	2100
Cu(I) 312.869	$4d\ ^4\mathbf{D}_{5/2}$ (8.9350)	$4p\ ^4\mathbf{P}_{3/2}$ (4.9734)	15000	700
Cu(I) 314.031	$4d\ ^2\mathbf{P}_{3/2}$ (8.7845)	$4p\ ^4\mathbf{P}_{5/2}$ (4.8876)	13000	600
Cu(I) 314.244	$4d\ ^4\mathbf{P}_{3/2}$ (8.9176)	$4p\ ^4\mathbf{P}_{3/2}$ (4.9734)	23000	1200
Cu(I) 314.682	$4d\ ^4\mathbf{P}_{1/2}$ (8.9122)	$4p\ ^4\mathbf{P}_{3/2}$ (4.9734)	15000	800
Cu(I) 316.967	$4d\ ^4\mathbf{G}_{7/2}$ (9.0634)	$4p\ ^4\mathbf{F}_{5/2}$ (5.1530)	14000	800
Cu(I) 317.568	$4d\ ^2\mathbf{G}_{7/2}$ (9.3242)	$4p\ ^2\mathbf{F}_{5/2}$ (5.4212)	11000	600
Cu(I) 323.390	$4d\ ^4\mathbf{D}_{5/2}$ (8.9350)	$4p\ ^4\mathbf{F}_{7/2}$ (5.1023)	22000	1500
Cu(I) 324.315	$4d\ ^4\mathbf{G}_{9/2}$ (8.9240)	$4p\ ^4\mathbf{F}_{7/2}$ (5.1023)	48000	2800
Cu(I) 324.753	$4p\ ^2\mathbf{P}_{3/2}$ (3.8166)	$4s\ ^2\mathbf{S}_{1/2}$ (0.0000)	530000	33000
Cu(I) 326.601	$4d\ ^2\mathbf{F}_{7/2}$ (9.3696)	$4p\ ^2\mathbf{F}_{7/2}$ (5.5746)	14000	800
Cu(I) 326.829	$4d\ ^2\mathbf{F}_{5/2}$ (8.9454)	$4p\ ^4\mathbf{F}_{5/2}$ (5.1530)	14000	800
Cu(I) 327.396	$4p\ ^2\mathbf{P}_{1/2}$ (3.7858)	$4s\ ^2\mathbf{S}_{1/2}$ (0.0000)	390000	27000
Cu(I) 327.981	$4p\ ^2\mathbf{F}_{5/2}$ (5.4212)	$4s\ ^2\mathbf{D}_{3/2}$ (1.6422)	20000	1200
Cu(I) 328.271	$4d\ ^2\mathbf{G}_{7/2}$ (8.9287)	$4p\ ^4\mathbf{F}_{5/2}$ (5.1530)	33000	2500
Cu(I) 329.054	$4d\ ^4\mathbf{F}_{9/2}$ (8.8387)	$4p\ ^4\mathbf{F}_{9/2}$ (5.0720)	55000	3900
Cu(I) 330.795	$4d\ ^4\mathbf{G}_{11/2}$ (8.8189)	$4p\ ^4\mathbf{F}_{9/2}$ (5.0720)	99000	6800
Cu(I) 331.722	$4d\ ^4\mathbf{F}_{9/2}$ (8.8387)	$4p\ ^4\mathbf{F}_{7/2}$ (5.1023)	19000	1500
Cu(I) 331.822	$6s\ ^4\mathbf{D}_{3/2}$ (9.3040)	$4p\ ^4\mathbf{F}_{7/2}$ (5.5687)	11000	800
Cu(I) 333.522	$4d\ ^2\mathbf{F}_{7/2}$ (8.8185)	$4p\ ^4\mathbf{F}_{7/2}$ (5.1023)	11000	900
Cu(I) 335.874	$4d\ ^4\mathbf{D}_{5/2}$ (8.9350)	$4p\ ^4\mathbf{F}_{3/2}$ (5.2447)	19000	1400
Cu(I) 337.459	$4d\ ^4\mathbf{P}_{3/2}$ (8.9176)	$4p\ ^4\mathbf{F}_{3/2}$ (5.2447)	13000	1100

(*continued*)

Table 1. Continued

Wavelength (nm)	Assignment		Relative intensity	
	Upper (eV)	Lower (eV)	Ar	He
Cu(I) 339.632	$4d\ ^{4}\mathbf{S}_{3/2}$ (8.8024)	$4p\ ^{4}\mathbf{F}_{5/2}$ (5.1530)	3400	200
Cu(I) 340.222	$4d\ ^{2}\mathbf{P}_{3/2}$ (9.3313)	$4p\ ^{2}\mathbf{P}_{3/2}$ (5.6882)	8100	400
Cu(I) 341.334	$4d\ ^{2}\mathbf{P}_{1/2}$ (9.3122)	$4p\ ^{2}\mathbf{P}_{1/2}$ (5.6882)	5600	300
Cu(I) 341.581	$4d\ ^{2}\mathbf{D}_{3/2}$ (9.3532)	$4p\ ^{2}\mathbf{D}_{3/2}$ (5.7246)	8600	500
Cu(I) 342.015	$4d\ ^{2}\mathbf{P}_{1/2}$ (9.3122)	$4p\ ^{2}\mathbf{P}_{3/2}$ (5.6882)	4300	200
Cu(I) 345.032	$4d\ ^{2}\mathbf{F}_{7/2}$ (9.3696)	$4p\ ^{2}\mathbf{D}_{5/2}$ (5.7773)	21000	1200
Cu(I) 345.285	$5s\ ^{2}\mathbf{D}_{3/2}$ (8.4272)	$4p\ ^{4}\mathbf{P}_{5/2}$ (4.8376)	8800	500
Cu(I) 345.785	$4p\ ^{4}\mathbf{P}_{3/2}$ (4.9734)	$4s\ ^{2}\mathbf{D}_{5/2}$ (1.3889)	1900	100
Cu(I) 345.941	$4d\ ^{4}\mathbf{F}_{5/2}$ (9.0884)	$4p\ ^{4}\mathbf{D}_{5/2}$ (5.5055)	1700	100
Cu(I) 346.544	$4d\ ^{2}\mathbf{D}_{5/2}$ (9.3540)	$4p\ ^{2}\mathbf{D}_{5/2}$ (5.7773)	7100	300
Cu(I) 347.175	$4d\ ^{2}\mathbf{D}_{5/2}$ (8.8148)	$4p\ ^{4}\mathbf{F}_{3/2}$ (5.2447)	4600	200
Cu(I) 347.457	$4d\ ^{4}\mathbf{F}_{3/2}$ (9.0899)	$4p\ ^{4}\mathbf{D}_{3/2}$ (5.5226)	17000	1000
Cu(I) 347.599	$4d\ ^{4}\mathbf{F}_{5/2}$ (9.0884)	$4p\ ^{4}\mathbf{D}_{3/2}$ (5.5226)		
Cu(I) 348.385	$4d\ ^{4}\mathbf{S}_{3/2}$ (8.8024)	$4p\ ^{4}\mathbf{F}_{3/2}$ (5.2447)	24000	1400
Cu(I) 348.756	$4d\ ^{2}\mathbf{P}_{3/2}$ (9.3313)	$4p\ ^{2}\mathbf{D}_{5/2}$ (5.7773)	3700	200
Cu(I) 349.096	$4d\ ^{2}\mathbf{F}_{5/2}$ (8.9454)	$4p\ ^{4}\mathbf{D}_{7/2}$ (5.3949)	1900	<100
Cu(I) 349.894	$6s\ ^{2}\mathbf{D}_{5/2}$ (9.3197)	$4p\ ^{2}\mathbf{D}_{5/2}$ (5.7773)	3300	200
Cu(I) 350.031	$4d\ ^{4}\mathbf{D}_{3/2}$ (9.0636)	$4p\ ^{4}\mathbf{D}_{3/2}$ (5.5226)	2800	200
Cu(I) 351.212	$4d\ ^{4}\mathbf{G}_{9/2}$ (8.9240)	$4p\ ^{4}\mathbf{D}_{7/2}$ (5.3949)	20000	1300
Cu(I) 351.702	$4d\ ^{2}\mathbf{F}_{5/2}$ (8.9454)	$4p\ ^{2}\mathbf{F}_{5/2}$ (5.4212)	4300	200
Cu(I) 352.001	$4d\ ^{4}\mathbf{F}_{3/2}$ (9.0899)	$4p\ ^{4}\mathbf{D}_{1/2}$ (5.5687)	14000	900
Cu(I) 352.423	$4d\ ^{4}\mathbf{F}_{7/2}$ (8.9382)	$4p\ ^{2}\mathbf{F}_{5/2}$ (5.4212)	25000	1600
Cu(I) 352.747	$4d\ ^{4}\mathbf{D}_{5/2}$ (8.9350)	$4p\ ^{2}\mathbf{F}_{5/2}$ (5.4212)	13000	800
Cu(I) 353.038	$4p\ ^{4}\mathbf{F}_{5/2}$ (5.1530)	$4s\ ^{2}\mathbf{D}_{3/2}$ (1.6422)	8000	400
Cu(I) 353.374	$4d\ ^{2}\mathbf{G}_{7/2}$ (8.9287)	$4p\ ^{2}\mathbf{F}_{5/2}$ (5.4212)	14000	900
Cu(I) 354.496	$4d\ ^{4}\mathbf{P}_{3/2}$ (8.9176)	$4p\ ^{2}\mathbf{F}_{5/2}$ (5.4212)	5000	300
Cu(I) 354.644	$4d\ ^{4}\mathbf{D}_{3/2}$ (9.0636)	$4p\ ^{4}\mathbf{D}_{1/2}$ (5.5687)	3500	100

excitation or stepwise deexcitation processes, the number density of copper in the plasma would determine their emission intensities. However, it is considered that the ionic lines requiring larger excitation energies can be excited mainly through collisions with fast electrons in the spark channel; therefore, the number density of fast electrons would be an important factor for determining their emission intensities. As shown in Fig. 4, the relative emission intensity of the ionic line in the helium plasma became larger compared with the argon plasma. The reason for this is that more fast electrons having enough energies to cause their ionization/excitation could survive in the helium spark channel due to the small interaction with helium atom. If the ratio of the sampling amount can be roughly estimated to be 0.1 from the data of the atomic resonance lines, the excitation efficiency of the ionic lines is 5 to 10 times higher in the helium plasma than that in the argon plasma.

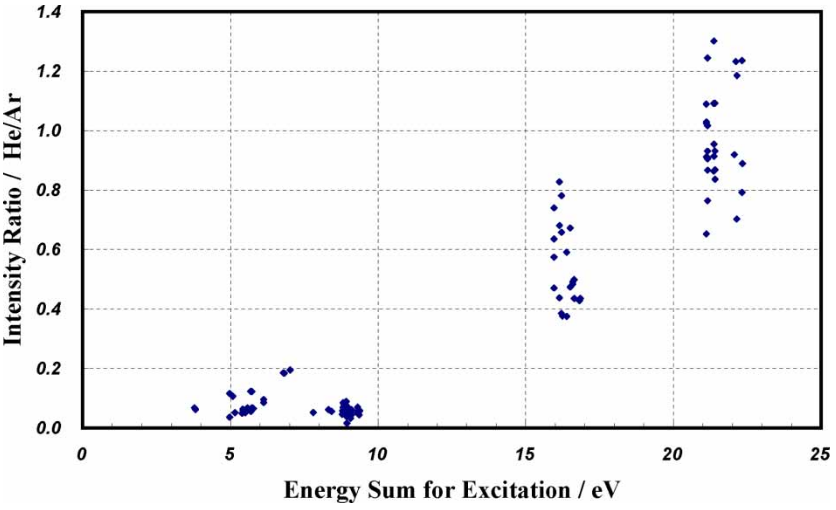

Figure 4. Variations in the intensity ratio of copper lines of the helium plasma to the argon plasma as a function of the excitation energy.

The analytical performance in atomic emission spectrometry can be estimated from the SBR of analytical lines under various discharge conditions. Table 2 summarizes the emission intensity as well as the SBR of some copper atomic and ionic lines selected. Although the emission intensities are

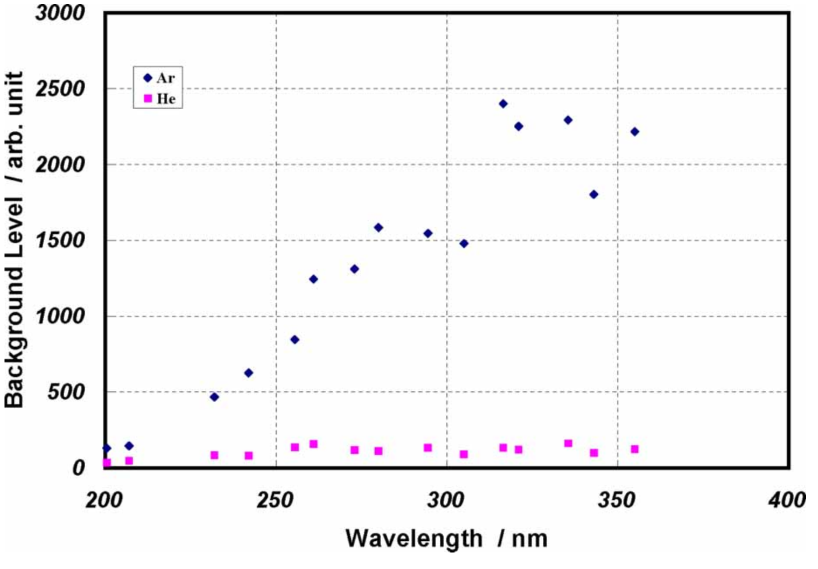

Figure 5. Wavelength dependence of the background level emitted from the argon and the helium plasmas.

Table 2. SBRs of several atomic and ionic copper lines emitted from the argon and the helium plasmas

Analytical line (nm)	Signal-to-background ratio (SBR)	
	Ar plasma	He plasma
Cu(II) 224.699	127.8	455.9
Cu(II) 229.436	77.1	248.5
Cu(II) 236.989	90.8	398.6
Cu(II) 240.334	12.6	107.9
Cu(II) 250.626	15.5	124.1
Cu(II) 254.480	26.7	213.8
Cu(I) 282.437	27.8	26.1
Cu(I) 296.117	26.7	25.7
Cu(I) 324.753	233.9	268.9
Cu(I) 327.396	174.3	219.1

generally small in the helium plasma, the SBRs are similar or better due to the very low background levels. Especially in the case of the ionic lines, the analytical performance of the helium plasma, based on the SBR, is superior to that of the argon plasma. When ionic lines have to be selected in practical applications, one should take into account the helium plasma.

CONCLUSIONS

The emission intensities of copper emission lines excited by spark discharge plasmas give different values when argon or helium is used as the surrounding gas. The atomic lines have much smaller intensities in the helium plasma than in the argon plasma, whereas little intensity difference for the ionic lines is observed between the argon and the helium plasmas. This effect is probably because the major excitation process for the ionic lines is different from the process for the atomic lines: various collisions with electrons as well as gas species or stepwise deexcitations determine excitations of the atomic lines, whereas collisions with fast electrons in the spark channel determine excitations of the ionic lines. The SBRs of some ionic copper lines are larger in the helium plasma compared with the argon plasma. Therefore, the helium plasma in some cases should be considered in analytical applications in SD-OES.

REFERENCES

1. Mandelstam, S. Excitation of the spectrum in a spark discharge. *Spectrochim. Acta* **1959**, *15*, 255–268.

2. Walters, J. P.; Malmstadt, H. V. Emission characteristics and sensitivity in a high-voltage spark discharge. *Anal. Chem.* **1965**, *37*, 1484–1503.
3. Walters, J. P. Historical advances in spark emission spectroscopy. *Appl. Spectrosc.* **1969**, *23*, 317–331.
4. Onodera, M.; Saeki, M.; Nishizaka, K.; Sakata, T.; Ono, J.; Fukui, I.; Imamura, N. Investigation on the metallographic analysis of small amount of aluminum in steel by emission spectrometric analysis. *Tetsu-to-Hagane* **1974**, *60*, 2002–2012.
5. Shibata, T.; Hamada, S.; Okuyama, Y.; Kashio, Y. Emission spectrometric analysis of sulfur free-cutting steel with high-energy pre-discharge method. *Tetsu-to-Hagane* **1979**, *65*, s986.
6. Matsumoto, Y. Determination of C, S, and O in steels by time-resolved atomic emission spectrometry. *Tetsu-to-Hagane* **1990**, *76*, 1387–1394.
7. Moore, C. E. *Atomic Energy Levels*; NBS Circular 467: Washington, DC, 1952.